MAGNETIC RESONANCE IN CHEMISTRY
Magn. Reson. Chem. **36**, 855–868 (1998)

^{2}H NMR lineshape analysis using automated fitting procedures based on local and quasi-global optimization techniques

Abil E. Aliev[1] and Kenneth D. M. Harris[2]*

[1] Department of Chemistry, University College London, 20 Gordon Street, London WC1H 0AJ, UK
[2] School of Chemistry, University of Birmingham, Edgbaston, Birmingham B15 2TT, UK

Received 21 December 1997; revised 14 May 1998; accepted 8 June 1998

ABSTRACT: A new approach is presented for the analysis of wideline ^{2}H NMR lineshapes, based on automated fitting of simulated spectra to experimental spectra using either 'downhill simplex' or simulated annealing algorithms. This approach provides an objective assessment of the level of agreement between experimental and simulated ^{2}H NMR spectra, and removes much of the subjectivity that is characteristic of the traditional approach involving trial-and-error variation of the parameters used in the simulation, followed by visual comparison between experimental and simulated ^{2}H NMR spectra to assess the quality of fit. Applications of our new approach are reported for the analysis of (i) static ^{2}H NMR powder patterns, (ii) the temperature dependence of ^{2}H NMR powder patterns in the intermediate motion regime (including the case of fitting experimental spectra with poor signal-to-noise ratio) and (iii) the dependence of quadrupole echo ^{2}H NMR spectra on the echo delay. Quantitative details relating to the dynamic properties of thiourea-d_4 in its pure crystalline phase and in the chlorocyclohexane–thiourea-d_4 inclusion compound are presented, in addition to the motion of the guest molecules in the benzenetricarbonylchromium-d_6–thiourea inclusion compound and the pyrazine-d_4–α-zirconium phosphate intercalation material. © 1998 John Wiley & Sons, Ltd.

KEYWORDS: lineshape analysis; deuterium NMR; automated fitting procedures; dynamics of solids; thiourea inclusion compounds

INTRODUCTION

^{2}H NMR spectroscopy has been applied widely to study molecular dynamics in a wide variety of anisotropic materials. Illustrative examples include phase transitions in rotator phase solids,[1,2] the dynamics of 'guest' molecules included in crystalline 'host' structures[3–6] and the motional properties of polymers and membranes.[7–9] Of the various wideline ^{2}H NMR techniques used to study the dynamic properties of solids, lineshape analysis of ^{2}H NMR powder patterns is undoubtedly the simplest and most widely applied. This approach is based on the fact that, when a ^{2}H nucleus undergoes reorientational motion on an appropriate time-scale, the ^{2}H NMR lineshape is altered in a well defined manner which can be interpreted in terms of the mechanism and rate of the dynamic process. When the rate of motion is 'intermediate' on the ^{2}H NMR time-scale (i.e. frequency of motion between about 10^3 and 10^8 s^{-1}), the appearance of the ^{2}H NMR spectrum depends critically upon the exact rate and geometry of the motion. It is generally straightforward to simulate the ^{2}H NMR spectrum theoretically for any proposed dynamic model for the ^{2}H nucleus, and this forms the basis of the standard procedure for interpretation of experimental ^{2}H NMR spectra. In particular, for a set of ^{2}H NMR spectra recorded as a function of temperature, the usual approach is to propose plausible mechanisms for the motion and then for each of these mechanisms (i) to simulate theoretically a set of ^{2}H NMR spectra for different values of the rate of motion and (ii) to decide which set of simulated ^{2}H NMR spectra is in best agreement with the set of experimental spectra. Once the correct dynamic model has been identified, comparison between the sets of simulated and experimental spectra allows the rate of motion to be determined as a function of temperature.

In terms of finding the simulated spectrum that best fits each experimental spectrum, the approach adopted so far has been based on trial-and-error variation of the parameters that define the dynamic model, coupled with an assessment of the quality of fit 'by eye' (i.e. visual comparison between simulated and experimental spectra). However, this procedure is highly subjective, and the fact that complex dynamic models require several parameters to be optimized simultaneously in fitting the simulated spectra to the experimental spectra renders the trial-and-error approach completely inefficient. Clearly, there is a pressing need for a more efficient, automated and robust approach for fitting simulated ^{2}H NMR spectra to experimental spectra.

* *Correspondence to*: K. D. M. Harris, School of Chemistry, University of Birmingham Edgbaston, Birmingham B15 2TT, UK
E-mail: k.d.m.harris@bham.ac.uk
Contract/grant sponsor: EPSRC.

 CCC 0749-1581/98/110855–14 $17.50

Examples of dynamic models that require simultaneous optimization of several parameters are often encountered in studies of macromolecules,[10] for which the motion is not necessarily based on a single correlation time. A distribution of correlation times may be considered by specifying a mean correlation time $\langle\tau_c\rangle$ and its log-Gaussian standard deviation σ—in this case, two variables (at least) are required in the fitting procedure. As a second example, molecules in solids often undergo reorientational motions about two or more axes, each characterized by a different rate constant, as well as small-amplitude librational motions that are rapid with respect to the ^{2}H NMR time-scale (and may vary in amplitude with temperature)[11,12]—in such cases, lineshape analysis requires simulation of the ^{2}H NMR spectra as a function of several independent variables, which significantly complicates the ability to find the best fits to the experimental spectra using the traditional approach.

In this paper, we describe a computational approach for ^{2}H NMR lineshape analysis, based on fitting simulated spectra to experimental spectra using either 'downhill simplex' or simulated annealing optimization algorithms. To illustrate the application of the technique, we consider the dynamic properties of the thiourea-d_4 molecules in the chlorocyclohexane–thiourea-d_4 inclusion compound and in the pure crystalline phase of thiourea-d_4, the dynamics of the guest molecules in the benzenetricarbonylchromium-d_6–thiourea inclusion compound [(η^6-C_6D_6)Cr(CO)$_3$–thiourea; abbreviated subsequently as BTCC-d_6–thiourea] and the dynamics of pyrazine-d_4 guest molecules in the pyrazine-d_4–α-zirconium phosphate intercalation material.

EXPERIMENTAL

^{2}H NMR spectra were recorded at 76.8 MHz on a Bruker MSL500 spectrometer and at 46.1 MHz on a Bruker MSL300 spectrometer, using standard Bruker 5 mm wideline probes. The stability and accuracy of the temperature controller (Bruker B-VT1000) were *ca.* ± 2 K. ^{2}H NMR spectra were recorded using the conventional quadrupole echo [$(90°)_\phi$–τ-$(90°)_{\phi\pm\pi/2}$–τ–acquire–recycle] pulse sequence,[13] with 90° pulse duration (t_p) in the range 2.0–3.5 μs, and echo delays $\tau = 13$ and 65 μs. Note that no spectral distortions occur for these values of τ; for the probes used, such distortions are observed only for $\tau < 10$ μs. The recycle delay was taken as *ca.* $10 \times T_1$, and ranged from 5 to 420 s depending on the sample and temperature. Phase cycling was employed to eliminate quadrature phase errors.

The chlorocyclohexane–thiourea-d_4 inclusion compound was prepared by slowly cooling a solution containing chlorocyclohexane and thiourea-d_4 dissolved in CH_3OD. After collecting the crystals, they were washed with 2,2,4-trimethylpentane to remove any chlorocyclohexane molecules adhering to their external surfaces. The sample prepared in this way was characterized by powder x-ray diffraction (verifying that the host structure was the same as that reported previously for chlorocyclohexane–thiourea[14]). Details of preparation and characterization of the BTCC-d_6–thiourea inclusion compound and the pyrazine-d_4–α-zirconium phosphate intercalation material are given in Refs 15 and 16, respectively.

^{2}H NMR LINESHAPE ANALYSIS

In modelling dynamic processes, each ^{2}H site involved in the motion can be defined by the Euler angles $\{\alpha, \beta, \gamma\}$, which specify the orientation (relative to a space fixed reference frame) of the principal axis system of the electric field gradient (EFG) tensor at the ^{2}H nucleus. We use $\mathbf{V}^{PAS}$ to denote the EFG tensor, in its principal axis system, at the ^{2}H nucleus. The properties and conventions relating to this tensor are as follows:

(a) The components of $\mathbf{V}^{PAS}$ are taken such that $|V_{zz}| \geqslant |V_{yy}| \geqslant |V_{xx}|$.
(b) The static quadrupole coupling constant χ is defined as eQV_{zz}/h (where Q is the electric quadrupole moment of the nucleus, $V_{zz} = \partial^2 V/\partial z^2$ is the largest principal component of the EFG tensor at the nucleus and e is the electronic charge).
(c) The static asymmetry parameter η is defined as $\eta = (|V_{yy}| - |V_{xx}|)/|V_{zz}|$, and is in the range $0 \leqslant \eta \leqslant 1$ [note that, as the $\mathbf{V}^{PAS}$ tensor is traceless, $V_{zz} = -(V_{xx} + V_{yy})$].

For the thiourea-d_4 molecule, the z-axis of $\mathbf{V}^{PAS}$ was taken to lie along the direction of the N—D bond and the y-axis of $\mathbf{V}^{PAS}$ was taken to be perpendicular to the plane of the molecule.[17]

For the BTCC-d_6 molecule, the z-axis of $\mathbf{V}^{PAS}$ was taken to lie along the direction of the C—D bond and the y-axis of $\mathbf{V}^{PAS}$ was taken to be perpendicular to the plane of the benzene ring.[18]

For the pyrazine-d_4 molecule, the z-axis of $\mathbf{V}^{PAS}$ was taken to lie along the direction of the C—D bond and the y-axis of $\mathbf{V}^{PAS}$ was taken to be perpendicular to the plane of the molecule. The direction of the y-axis of $\mathbf{V}^{PAS}$ was determined from spectral simulations in the intermediate motion regime (see also Ref. 17) for $\gamma = 0°$ (y-axis of $\mathbf{V}^{PAS}$ perpendicular to the molecular plane) and $\gamma = 90°$ (y-axis of $\mathbf{V}^{PAS}$ in the molecular plane) and comparing the results with the experimental spectrum recorded at 263 K. For $\gamma = 90°$ the width of the simulated powder pattern is less by *ca.* 10% than the width of the experimental powder pattern, whereas for $\gamma = 0°$ the simulation adequately reproduces the width and other features of the powder pattern (see Applications).

The first step of ^{2}H NMR lineshape analysis involves finding values of static quadrupole interaction parameters—the static quadrupole coupling constant (χ) and the static asymmetry parameter (η)—that best fit the experimental spectrum in the static (slow motion) regime. These values are then used as the static param-

eters χ and η in simulations when a dynamic model is considered.

In many cases, rapid (i.e. frequency greater than *ca.* 10^8 s^{-1}) small-amplitude motions occur in addition to the main dynamic process, and influence the ^{2}H NMR lineshape to some extent. In general, it is not necessary (and not convenient) to introduce these motions explicitly within the dynamic model used for simulation of the ^{2}H NMR spectrum, but rather to subsume the effects of these motions within the quadrupole interaction parameters used in the simulations. This is done using a motionally averaged ('effective') quadrupole coupling constant (denoted χ^*) and a motionally averaged ('effective') asymmetry parameter (denoted η^*), rather than the true static quadrupole coupling constant (χ) and the true static asymmetry parameter (η). The variation in the amplitude of rapid small-amplitude motions with temperature may be taken into account readily by allowing χ^* and η^* to be temperature dependent. In many cases, the values of χ^* and η^* may be computed directly from knowledge of the amplitude of these rapid small-amplitude motions, allowing only one additional parameter (i.e. amplitude), rather than two parameters (i.e. χ^* and η^*), to be varied in the lineshape fitting procedure.

In the present work, simulations of quadrupole echo ^{2}H NMR spectra in the intermediate motion regime were obtained using the modified version of the TURBOPOWDER program.[19] Simulations of static ^{2}H NMR powder patterns were carried out using the modified version of the POWPAT program.[20] The lineshape simulations take into account distortions in the intensities of shoulders in the ^{2}H NMR spectrum arising from finite pulse power.[21] The number of crystallite orientations considered was typically between 80 and 400, giving 'smooth' simulated ^{2}H NMR powder patterns. Spectrum widths were in the range 180–500 kHz with 200–1024 data points.

AUTOMATED PROCEDURES FOR FITTING SIMULATED SPECTRA TO EXPERIMENTAL SPECTRA

To assess the level of agreement between experimental and simulated ^{2}H NMR lineshapes (either for a static powder pattern or for a powder pattern influenced by molecular motion), we have used a merit function (*R*-factor) that provides a point-by-point comparison between corresponding digitised data points in the experimental and simulated ^{2}H NMR spectra:

$$R = \frac{1}{N} \sum_{i=1}^{N} (I_i^{\mathrm{exp}} - I_i^{\mathrm{calc}})^2$$

where I_i^{exp} is the intensity of the ith digitized data point in the experimental ^{2}H NMR spectrum ($i = 1, 2, \ldots, N$) and I_i^{calc} is the intensity of the ith digitized data point in the simulated ^{2}H NMR spectrum. In all cases discussed here, the experimental intensities I_i^{exp} were normalized, prior to any fitting procedures, such that each spectrum has the same maximum value of I_i^{exp}. The above definition of the *R*-factor assumes that the experimental errors in the measurement of each data point are independent of each other and equal to each other.

As discussed above, in order to obtain satisfactory agreement between experimental and simulated ^{2}H NMR spectra, it is often necessary to optimize several parameters that define the dynamic process. In general, each value of I_i^{calc} can be regarded as a function of the set (denoted $\mathbf{X}$) of the M variables that are allowed to refine in the fitting procedure: $\mathbf{X} = \{x_1, x_2, \ldots, x_M\}$. The automated fitting procedures that we employ here adjust the variables in the set $\mathbf{X}$ in order to achieve the minimum value of R, corresponding to the best fit between experimental and simulated spectra (subject to the constraints and approximations inherent within the model and the experimental errors contained within the experimental data). We considered two different approaches for achieving this multi-dimensional optimization: (i) a downhill simplex method[22,23] and (ii) a simulated annealing algorithm.[24]

The downhill simplex method invokes a simple algorithm for minimization of R. It is particularly straightforward in implement, as it requires only evaluation of the function of interest (i.e. simulation of spectra for a set of variables) and does not require evaluation of derivatives (unlike more sophisticated methods for minimization). However, as with any algorithm based on minimization, there is the potential danger that the calculation finds a local minimum in R, rather than the global minimum. The more robust, quasi-global optimization approach based on a simulated annealing algorithm allows this problem to be overcome.

The simulated annealing algorithm explores parameter space using the well known Metropolis sampling algorithm,[25] which operates as follows. Starting from an initial set of parameters $\mathbf{X}_1$ (based on some appropriate initial 'guess'), a sequence of parameter sets $\mathbf{X}_j$ is then generated. Importantly, each new parameter set ($\mathbf{X}_{j+1}$) in not generated 'from scratch,' but is derived from the previous parameter set ($\mathbf{X}_j$). The process for generating the parameter set $\mathbf{X}_{j+1}$ from the set $\mathbf{X}_j$ (termed a 'move') comprises the following steps.

1. Each parameter within the set $\mathbf{X}_j$ is subjected to a random 'displacement' to generate a new 'trial' value, giving rise to a trial parameter set $\mathbf{X}_j^{\mathrm{trial}}$. The displacement in the value of each parameter is constrained to lie within specified maximum and minimum bounds, which may be chosen to be different for each parameter. Furthermore, the maximum displacement may be taken as a function of the control parameter T (see below), such that the maximum allowed displacement decreases as T decreases. The value of the merit function R for the trial set of parameters $\mathbf{X}_j^{\mathrm{trial}}$ is then calculated.
2. The trial parameter set $\mathbf{X}_j^{\mathrm{trial}}$ is then accepted or rejected on the basis of the difference (Z) between its value of R and the value of R for the previous parameter set $\mathbf{X}_j$:

$$Z = R(\mathbf{X}_j^{\mathrm{trial}}) - R(\mathbf{X}_j)$$

If $Z \leqslant 0$, the trial parameter set is accepted as the new set (i.e. $\mathbf{X}_{j+1} = \mathbf{X}_j^{\text{trial}}$). If $Z > 0$, however, the trial set is accepted as the new set (i.e. $\mathbf{X}_{j+1} = \mathbf{X}_j^{\text{trial}}$) with probability $\exp(-Z/S)$ and rejected with probability $1 - \exp(-Z/S)$, where S represents an appropriate scaling of Z and can be regarded as proportional to an effective 'temperature' T. If the trial set of parameters $\mathbf{X}_j^{\text{trial}}$ is rejected, the new set $\mathbf{X}_{j+1}$ is taken to be the same as the previous set (i.e. $\mathbf{X}_{j+1} = \mathbf{X}_j$).

Steps 1 and 2 are repeated to generate a Markov chain of parameter sets $\mathbf{X}_{j+2}$, $\mathbf{X}_{j+3}$, $\mathbf{X}_{j+4}$, ..., $\mathbf{X}_F$. In the simulated annealing approach, an annealing schedule is applied, involving a gradual reduction of T as the calculation proceeds. By decreasing T sufficiently slowly, the simulated annealing technique leads, in principle, to the region of parameter space containing the lowest minimum in the merit function R. In our calculations, T was reduced by a factor of 0.85 (see Ref. 26) every 600–1000 moves. Starting values of T were chosen between 20 and 300 K. Note that in the limit $T \to 0$, the simulated annealing algorithm becomes equivalent to the downhill simplex method.

In the present work, the downhill simplex and simulated annealing algorithms were combined with the modified TURBOPOWDER and POWPAT programs used for simulation of ^{2}H NMR lineshapes. Our FORTRAN77 code was compiled on the following platforms: Silicon Graphics R8000/R8010 (90 MHz), Silicon Graphics R4400/R4010 (200 MHz), Silicon Graphics R4400/R4010 (150 MHz), Hewlett-Packard 9000/712 (80 MHz) and IBM PC (Pentium 120 MHz). In this paper, we illustrate the applications of these approaches for the analysis of (i) static ^{2}H NMR powder patterns, (ii) the temperature dependence of ^{2}H NMR powder patterns in the intermediate motion regime (including the case of fitting experimental spectra with poor signal/noise ratio) and (iii) the dependence of quadrupole echo ^{2}H NMR spectra on the echo delay.

APPLICATIONS

Fitting ^{2}H NMR powder patterns for static systems

The fitting procedures described above were applied to analyse the ^{2}H NMR spectra of thiourea-d_4 at 228 K and the chlorocyclohexane–thiourea-d_4 inclusion compound at 233 K. In both cases,[14,27] there are two crystallographically inequivalent ^{2}H environments, which we denote as 'axial' (D_{ax}) and 'equatorial' (D_{eq}). The N—D bond for the axial deuterons forms an angle $\beta_{ax} \approx 180°$ with the axis of the C=S bond, whereas the N—D bond for the equatorial deuterons forms an angle $\beta_{eq} \approx 60°$ with the axis of the C=S bond. Therefore, the fitting procedure requires optimization of two pairs of quadrupole interaction parameters, χ_{ax} and η_{ax} for the axial deuterons and χ_{eq} and η_{eq} for the equatorial deuterons.

In addition to χ and η, two other parameters, the line-broadening factor (L), applied as a Lorentzian broadening, and the 90° pulse duration (t_p), were also

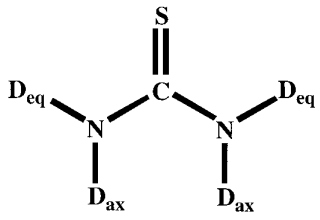

optimized in the spectral simulations. The line-broadening factor accounts for the intrinsic width of each line contributing to the powder pattern, and incorporates effects due to dipolar interactions between the ^{2}H nucleus and neighbouring nuclei of non-zero spin, field inhomogeneity and magnetic susceptibility, all of which are difficult to assess directly from experiment. The 90° pulse duration, on the other hand, is usually determined experimentally for a reference sample with a strong ^{2}H NMR signal [e.g. D_2O or deuterated poly(methyl methacrylate)] and is included as a parameter in spectral simulations to take into account distortions due to power roll-off effects.[21] It is important to note that the 'effective' pulse duration in the experiment for the sample of interest may be different from the 90° pulse duration measured for the reference sample, owing to differences in the dielectric properties of these samples. Furthermore, it has been shown[28] that because the load characteristics of probes are not purely resistive, better fits to experimental spectra can sometimes be achieved using an 'effective' pulse duration that is longer than the pulse duration determined experimentally. For these reasons, the parameters L and t_p were optimized together with χ and η in the fitting procedure. As L and t_p may be regarded as 'correction' factors, their optimization will mainly influence the overall quality of fit, without necessarily influencing the best-fit values of the quadrupole interaction parameters χ and η obtained in the fitting procedure.

Both downhill simplex and simulated annealing techniques were applied in the analysis of thiourea-d_4 and chlorocyclohexane–thiourea-d_4. The number of evaluations of the R factor was approximately 800 for the downhill simplex calculation and 58 000 for the simulated annealing calculation, corresponding to total computing times of *ca.* 0.3 and 24.5 h, respectively, on the Hewlett-Packard 9000/712 workstation. The results of the lineshape fitting are shown in Fig. 1 and the optimum values of the parameters are given in Table 1. The best-fit values of the parameters were found to be not particularly sensitive to the initial values used in the calculations—the quality of the initial guess is therefore not critical. Furthermore, the best-fit values found by the downhill simplex and simulated annealing techniques are similar. The quadrupole interaction parameters determined for the axial deuterons are in close agreement with those reported previously[27] from single-crystal ^{2}H NMR studies of thiourea-d_4 at 120 K ($\chi_{ax} = 212 \pm 3$ kHz; $\eta_{ax} = 0.154 \pm 0.007$). For the equatorial deuterons, the deviations from the values reported previously ($\chi_{eq} = 207 \pm 3$ kHz; $\eta_{eq} = 0.180 \pm 0.016$) are larger. In principle, values of the anisotropic tensor

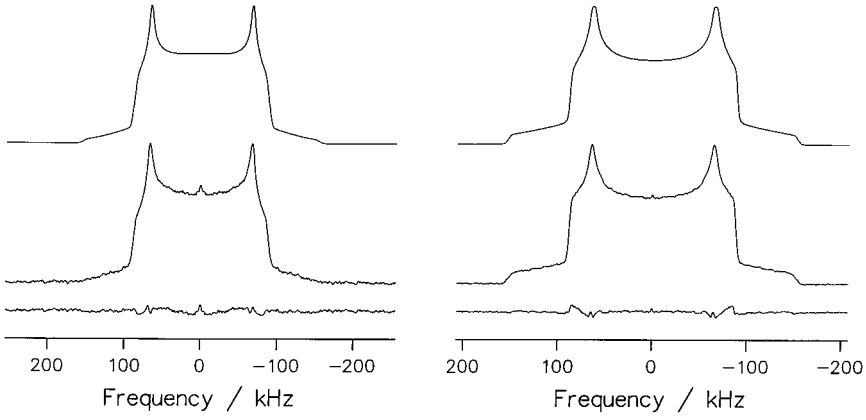

Figure 1. Best fits of simulated ^{2}H NMR spectra to experimental ^{2}H NMR spectra for pure crystalline thiourea-d_4 (left) and the chlorocyclohexane–thiourea-d_4 inclusion compound (right). Top trace, simulated spectrum; middle trace, experimental spectrum; bottom trace, difference between simulated and experimental spectra. The experimental spectra were recorded using the following conditions. Thiourea-d_4: 46.1 MHz; 228 K; $t_p = 3.4$ μs; $\tau = 13$ μs. Chlorocyclohexane–thiourea-d_4: 76.8 MHz; 233 K; $t_p = 2.4$ μs; $\tau = 13$ μs. The truncated narrow peak at zero frequency in the experimental spectra probably arises from residual amounts of CH_3OD (the solvent of crystallization). This part of the spectrum was not considered in the fitting procedure. The best-fit simulated spectra were obtained using the POWPAT program combined with the simulated annealing algorithm. The optimum values of the parameters in each case are shown in Table 1.

components determined for a single crystal and a polycrystalline sample may differ, as systematic errors may be introduced in determining the orientation dependence of the bulk magnetic susceptibility of a single crystal (such orientation dependence is averaged out in the case of a polycrystalline sample)—a similar problem has been demonstrated in determining the principal components of the shielding anisotropy tensor.[29] However, in the case of thiourea-d_4, the significant difference in the values of χ_{eq} and η_{eq} between the present work and Ref. 27 is probably due to slight differences in the nature of rapid small-amplitude librational motions at 228 and 120 K [we note also that several phase transitions occur in solid thiourea between these temperatures (at 169, 176, 190 and 202 K[27])]. The ways in which χ and η are influenced by these motions depend on the angle between the axis of libration and the N—D bond direction (strictly the z-axis of $\mathbf{V}^{PAS}$), which in general should be different for the axial and equatorial deuterons. For example, an increase of the amplitude of libration about the C=S bond on increasing temperature is expected to cause a substantially greater change in the values of χ^*_{eq} and η^*_{eq} than the values of χ^*_{ax} and η^*_{ax} (which will remain almost unchanged).

Table 1. Parameters for the best-fit simulated ^{2}H NMR spectra shown in Fig. 1[a]

Parameter	Thiourea-d_4	Chlorocyclohexane–thiourea-d_4
χ_{ax} (kHz)	210.1	207.0
η_{ax}	0.154	0.142
χ_{eq} (kHz)	204.1	202.4
η_{eq}	0.130	0.169
L (Hz)	1130	1420
t_p (μs)	3.48	2.46
R	1.24	1.29

[a] In the fitting procedure, the fractional convergence tolerance in the merit function R was 10^{-6}. The estimated uncertainties in the values of the best-fit parameters are $\Delta\chi \approx \pm 0.5$ kHz, $\Delta\eta \approx \pm 0.002$, $\Delta L \approx \pm 15$ Hz, $\Delta t_p \approx \pm 0.01$ μs (L denotes the Lorentzian broadening factor and t_p denotes the 90° pulse duration).

Fitting ^{2}H NMR powder patterns for dynamic systems in the intermediate motion regime

^{2}H NMR spectra recorded for thiourea-d_4 at temperatures from 263 to 333 K (Fig. 2) are clearly not static powder patterns, although the total widths of the spectra recorded at 323 and 333 K are only slightly (*ca.* 3%) less than that of the 'static' spectrum recorded at 228 K. The 'inner' powder pattern with intensity maxima at ±16.5 kHz and shoulders at ±99.5 kHz confirms the existence of deuterons undergoing substantial motion at temperatures in the range 263–333 K. In this temperature range, the lineshape can be interpreted as a superposition of two powder patterns (one similar in appearance to the powder pattern of a static system). The ^{2}H NMR spectra in the range 263–333 K have been simulated successfully on the basis of a dynamic model comprising a two-site π jump motion of the thiourea molecule about its C=S axis, together with rapid small-amplitude librational motions (the amplitude of which increases as temperature is increased).

In principle, the librational motions can be decomposed into three orthogonal components: (i) libration about an axis perpendicular to the molecular plane, (ii) libration about an axis parallel to the vector between the two nitrogen atoms in the molecule and (iii) libration about the C=S bond. In principle, these motions could be incorporated explicitly into the analysis, although this would require an appropriate potential function for the librational motions to be specified and the amplitudes of each of the components (i)–(iii) to be optimized as a function of temperature. In the present

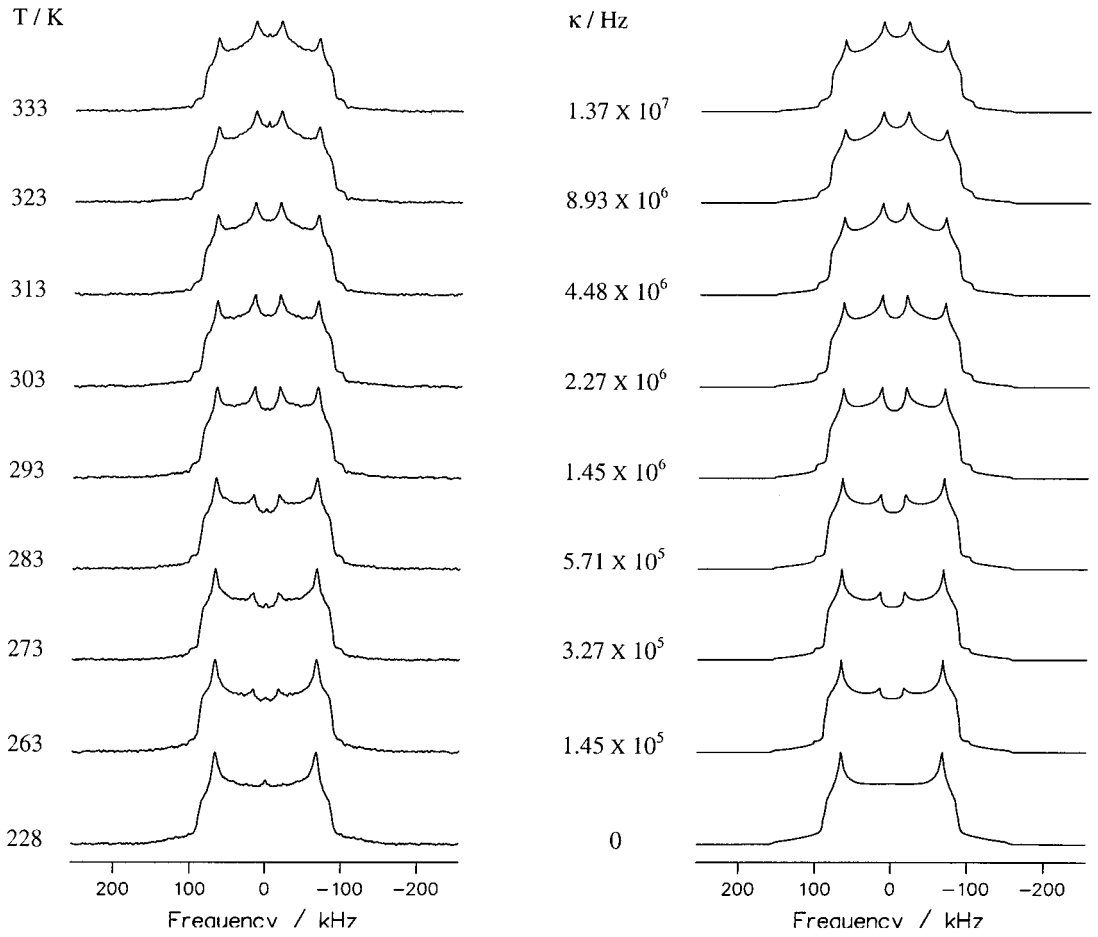

Figure 2. Left: experimental ^{2}H NMR spectra recorded at 46.1 MHz for pure crystalline thiourea-d_4 with $\tau = 13$ μs and $t_p = 3.4$ μs. The temperature at which each spectrum was recorded is shown. The truncated narrow peak at zero frequency in the experimental spectra probably arises from residual amounts of CH_3OD (the solvent of crystallisation). This part of the spectrum was not considered in the fitting procedure. Right: best-fit simulated ^{2}H NMR spectra calculated for the two-site π jump motion discussed in the text. The optimum rate (κ) of this jump motion is shown in each case. Best-fit simulated spectra were obtained using the TURBOPOWDER program combined with the downhill simplex optimization algorithm. The optimum values of the parameters are shown in Table 3.

work, we simplified the analysis by considering only the major component of the librational motion. According to neutron diffraction studies[30] at ambient temperature, motion (ii) has the largest amplitude ($\pm 11°$) and can be described by a rapid libration between azimuthal extrema $\pm\Phi$ (the centre of this range corresponds to the 'equilibrium' orientation of the thiourea molecule in the crystal). All orientations inside this range are assumed to be equally populated [i.e. the potential function $U(\Phi)$ is assumed to be constant]. On this basis, values of χ^* and η^* for axial and equatorial deuterons can be determined using the formalism developed in Ref. 31 as a function of one parameter only (the angle Φ) on the assumption that the values of the static quadrupole interaction parameters χ and η determined at 228 K (Table 1) correspond to the limiting behaviour as $\Phi \rightarrow 0$. This approach allows approximate values of χ^* and η^* for the axial and equatorial deuterons to be estimated at each temperature *by optimizing only one parameter.*

Lineshape simulations for the two-site π jump motion of the thiourea molecule about its C=S axis, combined with the librational motion discussed above, involved optimization of three parameters: the jump frequency κ for the two-site π jump motion, the libration amplitude Φ (as discussed above) and the angle β_{eq} between the C=S bond direction and the N—D_{eq} bond direction (strictly the z-axis of $\mathbf{V}^{PAS}$). Optimization of the angle β_{eq} is necessitated by the fact that the frequency separation between the 'inner' intensity maxima in the spectral simulations depends critically on the value of β_{eq}, and the possibility that β_{eq} exhibits some temperature dependence cannot be excluded. In our calculations, the angle β_{ax} was fixed at 178.5°, based on the value obtained from neutron diffraction studies[30] (tests showed that variation of β_{ax} by as much as $\pm 3°$ gives no perceptible change in the simulated ^{2}H NMR spectrum).

The downhill simplex algorithm was chosen for optimization in this case. The number of evaluations of the R-factor required to find the optimum solution was typically between 200 and 400. Typical computation times for each evaluation of the R-factor in the intermediate motion regime are summarized for different types of workstation in Table 2 [we note that simulation of

Table 2. Typical computation times (in seconds) for evaluation of the merit function R in the intermediate motion regime for different types of computer workstation used in this work[a]

Workstation	$N_c = 100$	$N_c = 200$	$N_c = 300$	$N_c = 400$
Silicon Graphics R8000 (90 MHz)	16	61	138	244
Silicon Graphics R4400 (200 MHz)	52	205	460	817
Silicon Graphics R4400 (150 MHz)	67	279	603	1086
Hewlett-Packard 9000/712 (80 MHz)	69	138	315	546
IBM PC (Pentium 120 MHz)	71	287	636	1136

[a] Calculations refer to the two-site π jump motion for the equatorial and axial deuterons in solid thiourea-d_4, with different numbers of crystallite orientations (N_c) considered in simulation of the ^{2}H NMR powder pattern. The number of data points considered was 848.

powder patterns (as required in the evaluation of R) is generally more time consuming for the intermediate motion regime than for the slow or rapid motion regimes].

The results obtained from fitting the simulated spectrum to the experimental spectrum at each temperature are shown in Fig. 2, and the optimum values of the parameters are given in Table 3. The best-fit values for β_{eq} between 263 and 333 K are in the range 61.1–61.3°, in excellent agreement with the value (61.24°) determined from neutron diffraction data for thiourea-d_4 at ambient temperature.[30] The corresponding angle determined from single-crystal ^{2}H NMR studies of thiourea-d_4 at 120 K is 62.8°.[27] On the assumption of Arrhenius behaviour for the temperature dependence of κ, the activation parameters for the two-site π jump motion about the C=S bond [determined from a graph of $\ln(\kappa/s)$ *vs.* $(T/K)^{-1}$] are $E_a = (47.8 \pm 1.1)$ kJ mol^{-1} and $A = (4.4 \pm 1.9) \times 10^{14}$ s^{-1}.

In a similar manner, we analysed the temperature dependence of the ^{2}H NMR spectra for the chlorocyclohexane–thiourea-d_4 inclusion compound in the range 276–363 K using the same dynamic model and fitting procedure. The results are shown in Fig. 3 and Table 4. The best-fit values for β_{eq} between 276 and 363 K are in the range 60.5–60.7°. The activation parameters for the two-site π jump motion about the C=S bond [determined from a graph of $\ln(\kappa/s)$ *vs.* $(T/K)^{-1}$] are $E_a = (37.4 \pm 1.0)$ kJ mol^{-1} and $A = (1.6 \pm 0.6) \times 10^{12}$ s^{-1}.

Fitting ^{2}H NMR powder patterns with poor signal-to-noise ratio for dynamic systems in the intermediate motion regime—assessment of the robustness of automated fitting procedures

We now consider ^{2}H NMR spectra of the pyrazine-d_4–α-zirconium phosphate intercalation material, which provide a test of the robustness of our automated fitting procedures for data with poor signal-to-noise ratio and with no prior knowledge of the motional model. Based on a qualitative inspection of the observed lineshapes, the following dynamic models for the pyrazine-d_4 guest molecules were considered:

(i) a dynamically homogeneous situation in which all pyrazine-d_4 molecules undergo a two-site π jump motion about the molecular C_2 axis, with equal populations for the two molecular orientations;
(ii) a dynamically homogeneous situation in which all pyrazine-d_4 molecules undergo a four-site $\pi/2$ jump motion about the molecular C_2 axis, with equal populations for the four molecular orientations;
(iii) a dynamically inhomogeneous situation comprising two types of guest molecules with different dynamic behaviour—molecules of type A undergo the two-

Table 3. Parameters for the best-fit simulated ^{2}H NMR spectra for thiourea-d_4 shown in Fig. 2[a]

T (K)	κ (s^{-1})	β_{eq} (°)	Φ (°)	χ^*_{ax} (kHz)	η^*_{ax}	χ^*_{eq} (kHz)	η^*_{eq}	R
263	1.45×10^5	61.17	5.3	208.8	0.142	203.3	0.129	2.10
273	3.27×10^5	61.17	8.0	207.5	0.137	203.1	0.127	1.82
283	5.71×10^5	61.22	9.2	206.9	0.134	202.9	0.126	1.50
293	1.45×10^6	61.23	10.3	206.2	0.132	202.8	0.125	1.38
303	2.27×10^6	61.30	10.4	206.1	0.131	202.7	0.125	1.02
313	4.48×10^6	61.30	12.5	204.5	0.124	202.4	0.123	1.16
323	8.93×10^6	61.34	13.6	203.6	0.120	202.2	0.121	1.68
333	1.37×10^7	61.39	13.9	203.4	0.119	202.1	0.121	0.91

[a] Three parameters (κ, β_{eq}, Φ) were optimized. The 'effective' static quadrupole interaction parameters (χ^*_{ax}, η^*_{ax}, χ^*_{eq} and η^*_{eq}) given in the table were determined from the optimized value of Φ. All spectra were calculated using a fixed Lorentzian broadening of 1130 Hz and a fixed 90° pulse duration of 3.48 μs.

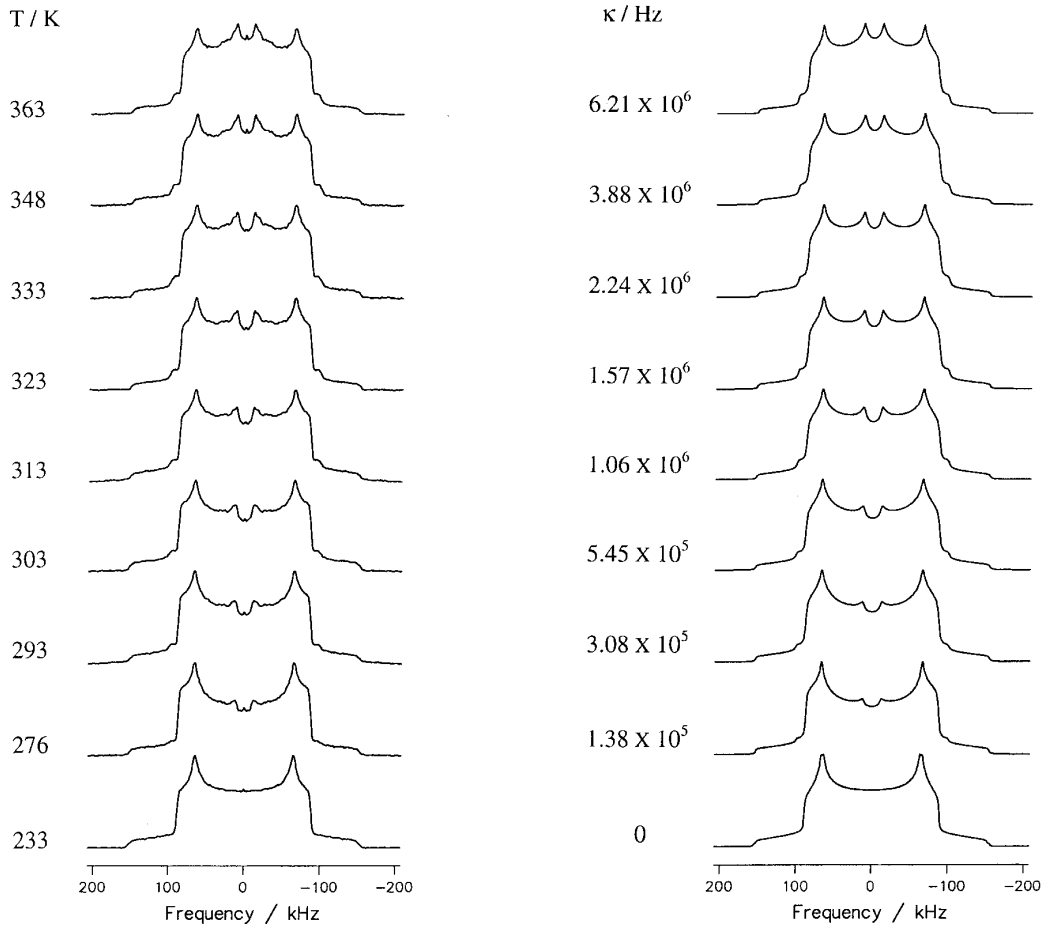

Figure 3. Left: experimental ^{2}H NMR spectra recorded at 76.8 MHz for the chlorocyclohexane–thiourea-d_4 inclusion compound with $\tau = 13$ μs and $t_p = 2.4$ μs. The temperature at which each spectrum was recorded is shown. The truncated narrow peak at zero frequency in the experimental spectra probably arises from residual amounts of CH_3OD (the solvent of crystallization). This part of the spectrum was not considered in the fitting procedure. Right: best-fit simulated ^{2}H NMR spectra calculated for the two-site π jump motion discussed in the text. The optimum rate (κ) of this jump motion is shown in each case. Best-fit simulated spectra were obtained using the TURBOPOWDER program combined with the downhill simplex optimization algorithm. The optimum values of the parameters are shown in Table 4.

site π jump motion described above [model (i)] and molecules of type B undergo the four-site $\pi/2$ jump motion described above [model (ii)]. The proportions (denoted p_A and p_B) of molecules of types A and B may take any value in the range 0–1 (note $p_B = 1 - p_A$).

For each motional model, the pyrazine-d_4 molecule was allowed to undergo rapid small-amplitude librations (between azimuthal extrema $\pm\Phi$) about the molecular C_2 axis at each site occupied during the jump process.

The static quadrupole interaction parameters ($\chi = 171.5$ kHz; $\eta = 0.074$) were determined by analysis

Table 4. Parameters for the best-fit simulated ^{2}H NMR spectra for the chlorocyclohexane–thiourea-d_4 inclusion compound shown in Fig. 3[a]

T (K)	κ (s^{-1})	β_{eq} (°)	Φ (°)	χ^*_{ax} (kHz)	η^*_{ax}	χ^*_{eq} (kHz)	η^*_{eq}	R
276	1.38×10^5	60.54	6.8	205.7	0.138	201.7	0.163	2.54
293	3.08×10^5	60.66	8.0	205.1	0.135	201.6	0.162	1.99
303	5.45×10^5	60.65	8.4	204.9	0.134	201.5	0.162	3.61
313	1.06×10^6	60.62	8.6	204.8	0.134	201.5	0.161	2.64
323	1.57×10^6	60.60	10.0	203.9	0.130	201.3	0.160	1.67
333	2.24×10^6	60.62	10.5	203.6	0.129	201.2	0.160	1.94
348	3.88×10^6	60.69	11.5	202.9	0.126	201.1	0.158	1.71
363	6.21×10^6	60.71	12.3	202.3	0.123	200.9	0.157	1.64

[a] Three parameters (κ, β_{eq}, Φ) were optimized. The 'effective' static quadrupole interaction parameters (χ^*_{ax}, η^*_{ax}, χ^*_{eq} and η^*_{eq}) given in the table were determined from the optimized value of Φ. All spectra were calculated using a fixed Lorentzian broadening factor of 1420 Hz and a fixed 90° pulse duration of 2.46 μs.

of the spectrum recorded at 183 K (Fig. 4) using the simulated annealing technique (a similar strategy is described in the first sub-section of Applications for thiourea-d_4). Attempts were made to fit the experimental spectrum recorded at 263 K using each of the dynamic models (i)–(iii). For models (i) and (ii), the following three parameters were allowed to vary in the fitting procedure: the rate constant κ for the jump motion, the angle Φ for the librational motion and the angle β between the molecular C_2 axis and the C—D bond vector (strictly the z-axis of $\mathbf{V}^{PAS}$). For model (iii), six parameters were allowed to vary in the fitting procedure: the rate constants κ_A and κ_B for the jump motions of molecules of types A and B, the angles Φ_A and Φ_B for the librational motions of molecules of types A and B, the angle β and the population p_A. For all three models, the spectra were fitted using the downhill simplex algorithm based on minimization of R, as described above.

As the data here have a comparatively poor signal-to-noise ratio, it is necessary to prevent the possibility that the fitting procedure attempts to fit features of the noise rather than the actual spectrum. In this regard, we considered the standard deviation (σ_d) determined for the difference spectrum (which in principle should contain only noise if the experimental spectrum is fitted perfectly) and the standard deviation (σ_s) determined from the first N' points in the actual experimental spectrum (here $N' = 256$, corresponding to baseline noise):

$$(\sigma_s)^2 = \frac{1}{N'-1}\sum_{i=1}^{N'}(I_i^{exp} - \langle I^{exp}\rangle)^2$$

where

$$\langle I^{exp}\rangle = \frac{1}{N'}\sum_{i=1}^{N'}(I_i^{exp})$$

The quality of fitting the simulated spectrum to the experimental spectrum should influence σ_d but does not influence σ_s. In our fitting calculations, σ_d was not allowed to be greater than σ_s. In the experimental spectra recorded at 263 and 298 K, the values of σ_s were 1.61 and 0.20, respectively.

The results of the automated fitting using the downhill simplex algorithm are shown in Table 5. At 263 K, model (i) fits the outer edges of the experimental spectrum reasonably well, but fails to fit the central part of the spectrum. Model (ii), on the other hand, gives a better fit for the central part of the spectrum and a poorer fit to the outer edges, but the R-factor is significantly lower than for model (i). Model (iii) adequately reproduces all the features of the experimental spectrum. Figure 5 shows the experimental spectrum at 263 K and the best-fit calculated spectra for models (ii) and (iii).

We also used model (iii) to fit the ^{2}H NMR spectrum recorded at 298 K (Fig. 6) using the downhill simplex algorithm. As shown in Table 5, the best-fit values of p_A and β are in close agreement with those found at 263 K, whereas the values of κ_A, κ_B, Φ_A and Φ_B are higher than those found at 263 K, as expected intuitively. Separate simulations using the best-fit values of the parameters shown in Table 5 indicate that the four-site $\pi/2$ jump motion (molecules of type B) contributes mainly to the narrow central component of the spectrum, whereas the two-site π jump motion (molecules of type A) contributes mainly to the wider parts of the powder pattern ('shoulders') in the frequency range *ca.* $\pm$75 kHz.

In all examples discussed above, the fitting procedures were based on minimization of R. In the present case for model (iii), the fitting procedures were also assessed for minimization of two other functions—σ_d (as defined above) and R' (the absolute deviation function). The definition of R' is

$$R' = \frac{1}{N}\sum_{i=1}^{N}|I_i^{exp} - I_i^{calc}|$$

As shown in Table 5, the values of the parameters obtained from minimization of R, R' and σ_d are in close agreement. The spread of the optimum values is larger for κ_B and Φ_B, probably reflecting the low population of molecules of type B and suggesting that the lineshape fitting is less sensitive to the parameters describing the motion of these molecules.

Clearly, a more detailed investigation of the existence and nature of the two dynamically distinct types of

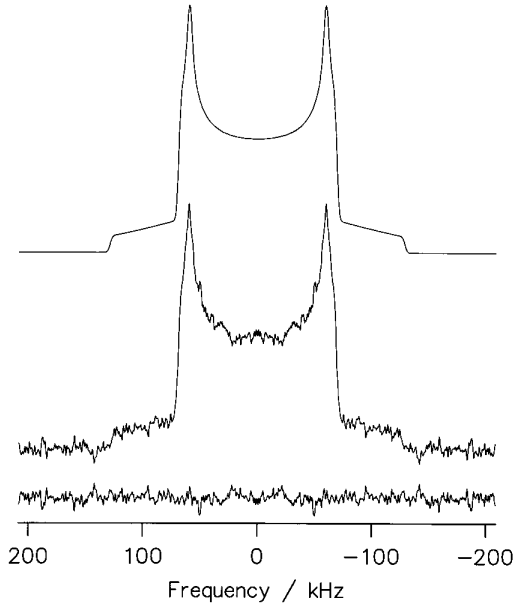

Figure 4. Experimental ^{2}H NMR spectrum for the pyrazine-d_4–α-zirconium phosphate intercalation material at 183 K (middle trace), best fit simulated ^{2}H NMR spectrum (top trace) and the difference between the simulated and experimental spectra (bottom trace). The experimental spectrum was recorded using the following conditions: 46.1 MHz; $t_p = 3.5$ μs; $\tau = 31$ μs. The best-fit simulated spectrum was obtained using the POWPAT program combined with the simulated annealing algorithm. The parameters corresponding to the best fit (with $R = 3.56$) are $\chi = 171.5 \pm 0.7$ kHz, $\eta = 0.074 \pm 0.005$, $L = 1050 \pm 30$ Hz and $t_p = 3.46 \pm 0.03$ μs.

Table 5. Parameters for the best-fit simulated ^{2}H NMR spectra for the pyrazine-d_4–α-zirconium phosphate intercalation material shown in Figs 5 and 6[a]

Model	T (K)	κ_A (s^{-1})	Φ_A (°)	κ_B (s^{-1})	Φ_B (°)	β (°)	p_A	R	R'	σ_d	Merit function minimized in fitting procedure	N_{it}	CPU time (s)
(i)	263	4.57×10^6	1.8	—	—	55.68	1	108.40	—	9.93	R	57	938
(i)	298	5.76×10^6	1.8	—	—	55.68	1	432.72	—	17.50	R	36	600
(ii)	263	—	—	3.95×10^4	1.9	55.41	0	6.94	—	3.35	R	208	2706
(ii)	298	—	—	7.17×10^4	1.8	55.76	0	3.76	—	2.73	R	151	1964
(iii)	263	1.27×10^6	11.8	5.76×10^5	0.5	56.03	0.72	2.63	—	1.63	R	456	9020
(iii)	298	1.37×10^7	14.0	1.54×10^6	6.3	55.48	0.74	0.06	—	0.27	R	312	6089
(iii)	263	1.32×10^6	11.9	5.63×10^5	1.1	56.02	0.73	—	—	1.61	σ_d	332	6509
(iii)	298	1.39×10^7	14.0	1.52×10^6	0.3	55.54	0.74	—	—	0.27	σ_d	358	6441
(iii)	263	1.56×10^6	11.9	5.68×10^5	0.7	56.02	0.77	—	1.29	1.64	R'	620	12 156
(iii)	298	1.49×10^7	15.0	1.43×10^6	5.2	55.96	0.74	—	0.19	0.29	R'	363	7015

[a] Three parameters (κ, Φ, β) were optimized for models (i) and (ii) and six parameters (κ_A, Φ_A, κ_B, Φ_B, β, p_A) were optimized for model (iii). All spectra were calculated using a fixed Lorentzian broadening factor of 1 kHz and a fixed 90° pulse duration of 3.5 μs. The number of iterations required for convergence of the downhill simplex algorithm is denoted N_{it}. All calculations were carried out on the Silicon Graphics R8000 workstation.

pyrazine-d_4 guest molecules within the α-zirconium phosphate host material requires the application of a range of other techniques, including ^{2}H T_1 measurements, and a full analysis of the dynamic properties of this system will be published in due course. Nevertheless, this example illustrates that our automated fitting procedure provides a robust approach for the analysis of ^{2}H NMR spectra with poor signal-to-noise ratios, even when complex models are required to describe the dynamics of the system.

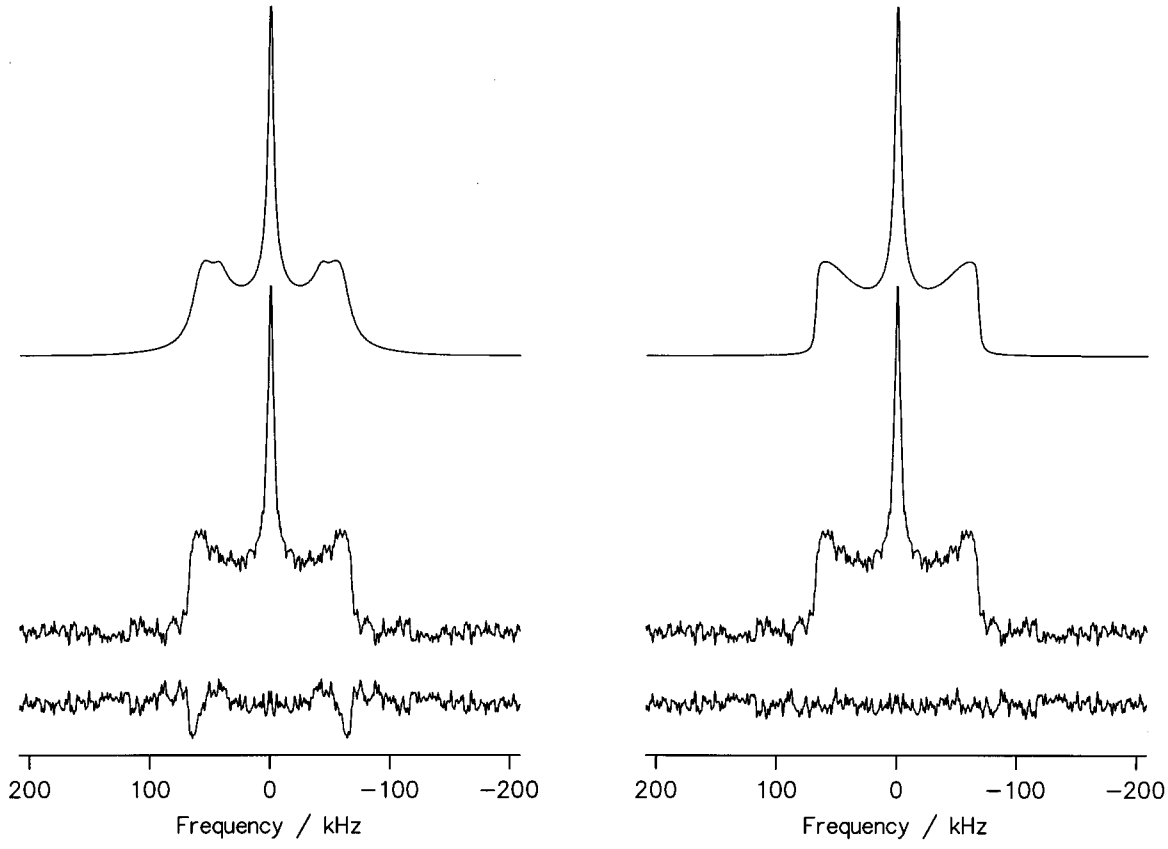

Figure 5. Experimental ^{2}H NMR spectrum for the pyrazine-d_4–α-zirconium phosphate intercalation material at 263 K (middle trace), best fit simulated ^{2}H NMR spectrum (top trace) and the difference between the simulated and experimental spectra (bottom trace). Left: results for model (ii). Right: results for model (iii). The experimental spectrum was recorded using the following conditions: 46.1 MHz; $t_p = 3.5$ μs; $\tau = 31$ μs. The best-fit simulated spectrum was obtained using the TURBOPOWDER program combined with the downhill simplex algorithm. The optimum values of the parameters are shown in Table 5.

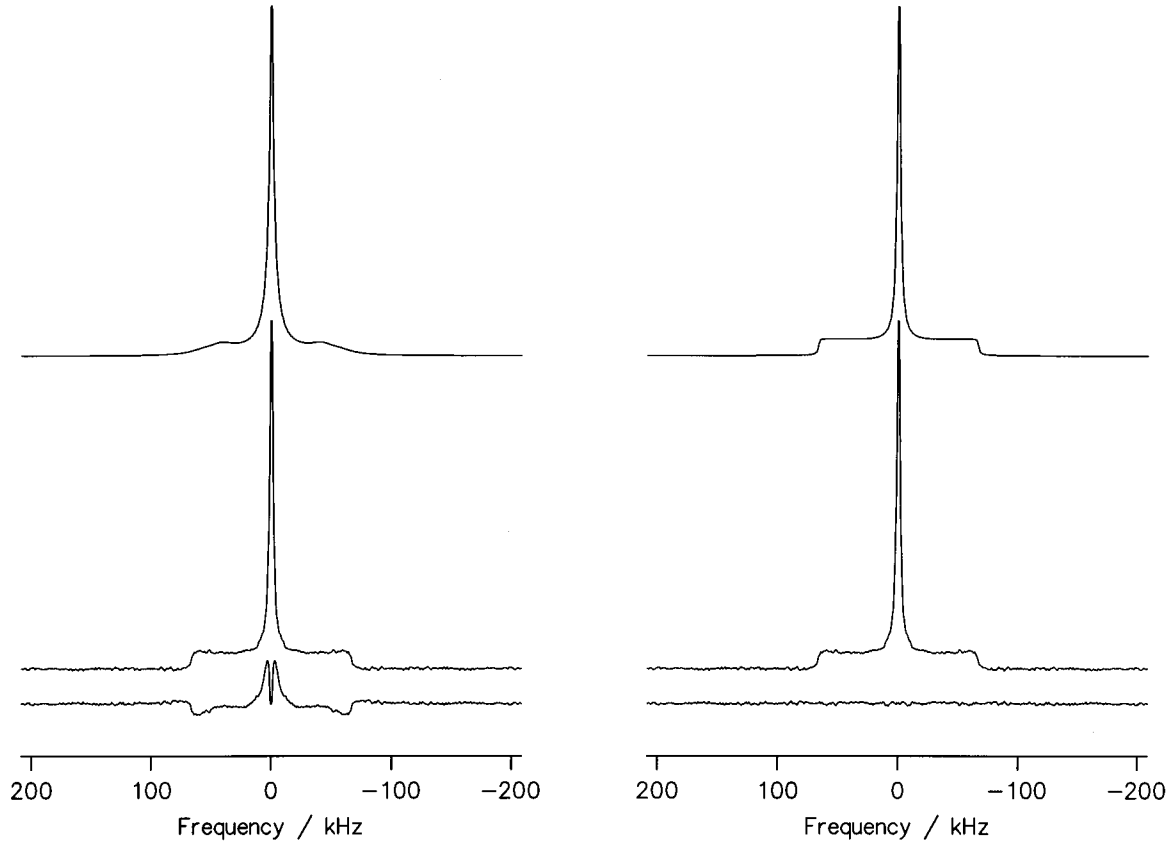

Figure 6. Experimental ^{2}H NMR spectrum for the pyrazine-d_4–α-zirconium phosphate intercalation material at 298 K (middle trace), best simulated ^{2} H NMR specrum (top trace) and the difference between the simulated and experimental spectra (bottom trace). Left: results for model (ii). Right: results for model (iii). The experimental spectrum was recorded using the following conditions: 46.1 MHz; $t_p = 3.5$ μs; $\tau = 31$ μs. The best-fit simulated spectrum was obtained using the TURBOPOWDER program combined with the downhill simplex algorithm. The optimum values of the parameters are shown in Table 5.

Fitting ^{2}H NMR spectra recorded as a function of echo delay (τ)

The amount of experimental ^{2}H NMR data available at each temperature can be expanded by measuring a set of spectra for n different values of the echo delay (τ) in the quadrupole echo pulse sequence. In certain cases, this approach may be essential for distinguishing different dynamic models that give rise to similar spectra for a particular value of τ. It is important to note that the n different spectra considered in this approach are not independent, as they all depend on the same dynamic model and are linked by the well defined τ dependence associated with this dynamic model. As such, the study of the τ dependence of the quadrupole echo lineshape greatly enhances the available data, without introducing any additional complexity to the dynamic model.

When the echo delay is short, the ^{2}H NMR lineshape is particularly sensitive to κ in the 'lower intermediate' motion regime, whereas when the echo delay is long, the ^{2}H NMR lineshape is particularly sensitive to κ in the 'upper intermediate' motion regime. In principle, the τ dependence of ^{2}H NMR spectra extends the range of rates of motion that can be investigated (although there is clearly a limitation on the maximum value of τ). For example, in favourable cases, rates in the fast range 10^8–10^9 s^{-1} can be studied using values of τ in the range 0.1–1 ms.[32]

In general, a set of n spectra (e.g. for the echo delays τ_1, τ_2, ..., τ_n at a given temperature) may be fitted simultaneously using an overall merit function (R_{total}) taken as the average of the merit functions for the n different spectra:

$$R_{total} = \frac{1}{n}\{R_1 + R_2 + \ldots + R_n\}$$

With this definition, in which each individual spectrum is equally weighted, we recall that the absolute intensity of each experimental spectrum is normalized independently.

To illustrate the application of our fitting procedures for a set of τ-dependent ^{2}H NMR spectra in the intermediate motion regime, we consider the BTCC-d_6–thiourea inclusion compound. Figure 7 shows the experimental ^{2}H NMR spectra (recorded with $\tau = 13$ and 65 μs) at 189 K. As shown recently,[15] changes in the ^{2}H NMR lineshape with temperature in the range 123–203 K and the temperature dependence of the ^{2}H

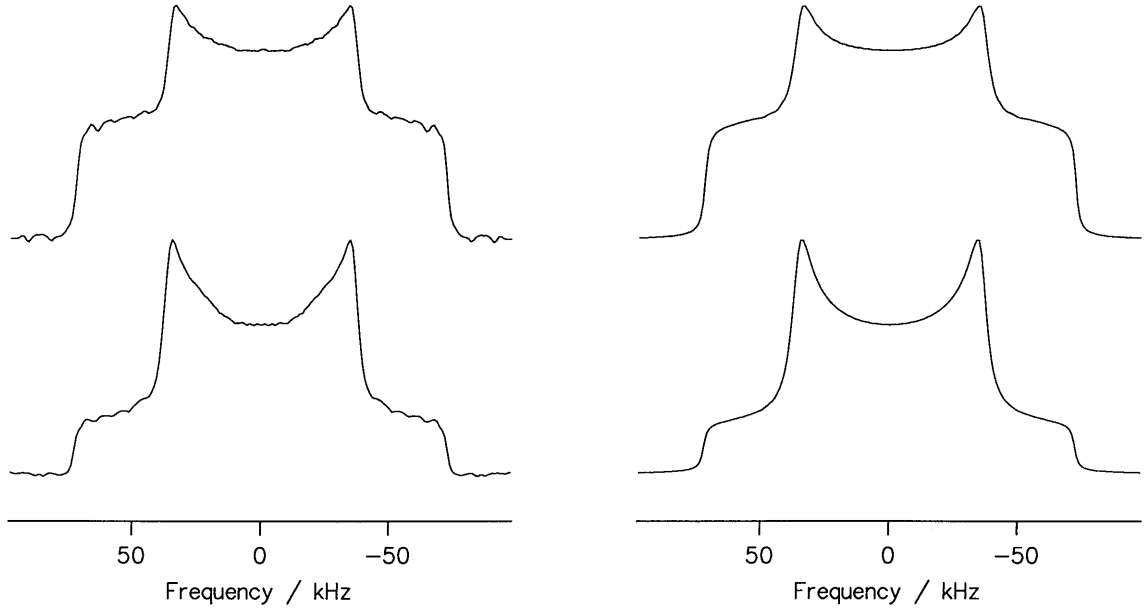

Figure 7. Left: experimental ^{2}H NMR spectra for BTCC-d_6–thiourea recorded at 189 K and 46.1 MHz using echo delays $\tau = 13$ μs (bottom trace) and 65 μs (top trace). The 90° pulse duration was $t_p = 2.0$ μs. Right: best-fit simulated ^{2}H NMR spectra for the dynamic model discussed in the text, obtained using the TURBOPOWDER program combined with the downhill simplex optimisation algorithm. The optimized parameters, corresponding to the best fit (with $R_{total} = 3.24$), are $\kappa = (5.31 \pm 0.02) \times 10^6$ s^{-1}, $L = (1040 \pm 20)$ Hz, $\chi = (181 \pm 1)$ kHz and $\eta = 0.064 \pm 0.003$.

NMR spin–lattice relaxation time in the range 173–363 K can be rationalized on the basis of a nearest neighbour six-site $2\pi/6$ jump model for the benzene moiety of BTCC-d_6 about its C_6 symmetry axis. In our previous work,[15] values of the static quadrupole coupling constant $\chi = 186$ kHz and static asymmetry parameter $\eta = 0.06$ were determined from the spectrum recorded at 103 K in the 'slow' motion regime by visual comparison between the simulated and experimental spectra. In the present work, χ and η were considered as variables in the optimization, together with the jump frequency κ and the line-broadening factor L. The results of the fitting procedure using the downhill simplex algorithm for optimization of the four parameters by fitting simulated spectra *simultaneously* to the experimental spectra recorded at 189 K for the echo delays $\tau = 13$ and 65 μs are shown in Fig. 7. The automated fitting procedure leads to a good simultaneous fit to both experimental spectra (recorded with different echo delays) for a single set of fitted parameters.

The analysis of the τ dependence of the quadrupole echo ^{2}H NMR spectra can be further extended by considering the integrated intensity of the spectrum as a function of τ. For the experimental spectra recorded at 189 K (with the same number of scans), the integrated intensity of the spectrum recorded with $\tau = 65$ μs is less by a factor of 61% than that for the spectrum recorded with $\tau = 13$ μs. For simulated spectra calculated using the best-fit parameters obtained above (but clearly without normalization of intensities), the integrated intensity of the spectrum recorded with $\tau = 65$ μs is less by a factor of 59% than that for the spectrum recorded with $\tau = 13$ μs. This close agreement between the experimental and simulated intensity loss factors gives further support to the proposed dynamic model.

We note that, in certain cases, anisotropic dipole–dipole interactions can affect the quadrupole echo ^{2}H NMR lineshape at higher values of τ, such that the effects of dynamic processes on the lineshape become obscured. In such cases, it is clearly not valid to interpret the τ dependence of the lineshape on the basis of dynamic processes alone. For thiourea-d_4, the anisotropic ^{14}N–^{2}H dipole–dipole interactions present problems in this regard,[33] and for this reason we have not studied the τ dependence of the ^{2}H NMR spectrum for thiourea-d_4, either in its pure crystalline phase or in the chlorocyclohexane–thiourea-d_4 inclusion compound. Similarly, for partially deuterated solids, the anisotropic ^{1}H–^{2}H dipole–dipole interactions can affect the quadrupole echo ^{2}H NMR lineshape at higher values of τ.[34] For the BTCC-d_6–thiourea inclusion compound discussed above, however, any effects due to anisotropic dipole–dipole interactions are negligible.

CONCLUSION

The examples presented here have demonstrated a new approach for the analysis of wideline ^{2}H NMR lineshapes, based on the application of automated fitting procedures involving downhill simplex and simulated annealing techniques. This strategy provides an objec-

tive assessment of the level of agreement between experimental and simulated ^{2}H NMR spectra, and removes much of the subjectivity that is characteristic of the traditional approach involving trial-and-error variation of parameters, coupled with visual comparison between experimental and simulated spectra. The success of the new strategy has been demonstrated for the extraction of parameters from 'static' ^{2}H NMR powder patterns, for the analysis of the temperature dependence of ^{2}H NMR powder patterns in the intermediate motion regime and for the analysis of the τ dependence of quadrupole echo ^{2}H NMR spectra. In addition to the examples presented here, the new approach has also been applied successfully to study the dynamic properties of the hydrogen bonding arrangement in a selectively deuterated sample of solid triphenylmethanol (Ph_3COD)[35] and the guest molecular dynamics in the dioctanoyl peroxide–urea inclusion compound[36] (in combination with incoherent quasi-elastic neutron scattering studies).

We now consider further improvements and developments of our automated approach. The main disadvantage of the simulated annealing technique is the large number of parameter sets that must be considered—as it is time consuming to compute even a single ^{2}H NMR powder pattern, the overall time required for the simulated annealing calculation may be excessive. One of the time-consuming stages in lineshape simulations for static systems is the calculation of the powder pattern using the Alderman, Solum and Grant tiling method for the evaluation of elliptic integrals.[37] Recently, however, novel approaches for calculation of static powder lineshapes have been suggested,[38,39] allowing a significant reduction of the calculation time. It is expected that these new approaches for calculating the powder pattern will greatly facilitate automated fitting based on the simulated annealing algorithm developed here.

Our future investigations will also consider other techniques for global optimization, including the application of genetic algorithms,[40–44] leading to a detailed assessment of the relative efficiencies of the genetic algorithm and simulated annealing techniques. Hybrid local search algorithms combining features of simulated annealing and genetic algorithms will also be considered.

It is clear that the techniques discussed here provide an objective assessment of the level of agreement between experimental and simulated ^{2}H NMR spectra, and remove much of the subjectivity associated with the traditional approach of comparing experimental and simulated ^{2}H NMR spectra 'by eye.' Furthermore, the automated nature of the new approach and the opportunity for simultaneous optimisation of several parameters greatly facilitate ^{2}H NMR lineshape analysis in cases with complex dynamic models.

Acknowledgements

Financial support from EPSRC (general support to K.D.M.H.) is gratefully acknowledged. The University of London Intercollegiate Research Service is thanked for the provision of facilities for solid-state NMR spectroscopy. We are grateful to Dr F. Guillaume for providing the sample of BTCC-d_6–thiourea, to Dr G. B. Hix for providing the sample of pyrazine-d_4–α-zirconium phosphate, to Professor R. G. Griffin for providing the TURBOPOWDER program and to Professor D. C. Clary for access to computing facilities.

REFERENCES

1. O. Pschorn and H. W. Spiess, *J. Magn. Reson.* **39**, 217 (1980).
2. A. E. Aliev and K. D. M. Harris, *Mendeleev Commun.* 153 (1993).
3. R. L. Vold, R. R. Vold and N. J. Heaton, *Adv. Magn. Reson.* **13**, 17 (1989).
4. J. A. Ripmeester and C. I. Ratcliffe, *Inclusion Compd.* **5**, 37 (1991).
5. G. L. Hoatson and R. L. Vold, in *NMR Basic Principles and Progress*, edited by P. Diehl, E. Fluck, H. Günther, R. Kosfeld and J. Seelig, Vol. 32, pp. 3–67. Springer, Berlin (1994).
6. R. R. Vold, in *Nuclear Magnetic Resonance Probes of Molecular Dynamics*, edited by R. Tycko, pp. 27–106. Kluwer, Dordrecht (1994).
7. J. Seelig, *Q. Rev. Biophys.* **10**, 353 (1977).
8. T. M. Alam and G. P. Drobny, *Chem. Rev.* **91**, 1545 (1991).
9. R. G. Griffin, *Methods Enzymol.* **72**, 108 (1991).
10. R. J. Schadt, E. J. Cain and A. D. English, *J. Phys. Chem.* **97**, 8387 (1993).
11. J. H. Ok, R. R. Vold and R. L. Vold, *J. Phys. Chem.* **93**, 7618 (1989).
12. S. J. Heyes and C. M. Dobson, *Magn. Reson. Chem.* **28**, S37 (1990).
13. J. H. Davis, K. R. Jeffrey, M. Bloom, M. I. Valic and T. P. Higgs, *Chem. Phys. Lett.* **42**, 390 (1976).
14. K. D. M. Harris and J. M. Thomas, *J. Chem. Soc., Faraday Trans.* **86**, 1095 (1990).
15. A. E. Aliev, K. D. M. Harris and F. Guillaume, *J. Chem. Res.* (*S*) 294 (1995).
16. G. B. Hix and K. D. M. Harris, *Eur. J. Solid State Inorg. Chem.* **34**, 589 (1997).
17. N. J. Heaton, R. L. Vold and R. R. Vold, *J. Am. Chem. Soc.* **111**, 3211 (1989).
18. A. E. Aliev, K. D. M. Harris and F. Guillaume, *J. Phys. Chem.* **99**, 1156 (1995).
19. R. J. Wittebort, E. T. Olejniczak and R. G. Griffin, *J. Chem. Phys.* **86**, 5411 (1987).
20. H. S. Story and D. Kline, Department of Physics, State University of New York at Albany (an extension of *QCPE 154* and *QCMP 56*).
21. M. Bloom, J. H. Davis and M. I. Valic, *Can. J. Phys.* **58**, 1510 (1980).
22. J. A. Nelder and R. Mead, *Comput. J.* **7**, 308 (1965).
23. W. H. Press, B. P. Flannery, S. A. Teukolsky and W. T. Vetterling, *Numerical Recipes—The Art of Scientific Computing*. Cambridge University Press, Cambridge (1989).
24. S. Kirkpatrick, *J. Stat. Phys.* **34**, 975 (1984).
25. N. Metropolis, A. Rosenbluth, M. Rosenbluth, A. Teller and E. Teller, *J. Chem. Phys.* **21**, 1087 (1953).
26. A. Corana, C. Marchesi and S. Ridella, *ACM Trans. Math. Software* **13**, 162 (1987).
27. D. E. O'Reilly, E. M. Peterson and Z. M. El Saffar, *J. Chem. Phys.* **54**, 1304 (1971).
28. J. Hirschinger, H. Miura, K. H. Gardner and A. D. English, *Macromolecules* **23**, 2153 (1990).
29. Z. Olender, R. Poupko, Z. Luz, B. Tesche, H. Zimmermann and U. Haeberlen, *J. Magn. Reson. A* **114**, 179 (1995).
30. M. M. Elcombe and J. C. Taylor, *Acta Crystallogr., Sect. A* **24**, 410 (1968).
31. P. A. Armstrong, A. T. Bell and J. A. Reimer, *Solid State NMR* **2**, 1 (1993).
32. K. Beshah, E. T. Olejniczak and R. G. Griffin, *J. Chem. Phys.* **86**, 4730 (1987).
33. T.-H. Lin and R. R. Vold, *J. Magn. Reson.* **113**, 271 (1995).
34. N. Boden and P. K. Kahol, *Mol. Phys.* **40**, 1117 (1980).
35. A. E. Aliev, E. J. MacLean, K. D. M. Harris, B. M. Kariuki and C. Glidewell, *J. Phys. Chem.* **102**, 2165 (1998).
36. P. Girard, A. E. Aliev, F. Guillaume, K. D. M. Harris, M. D. Hollingsworth, A. J. Dianoux and P. Jonsen, *J. Chem. Phys.* **109**, 4078 (1998).

37. D. W. Alderman, M. S. Solum and D. M. Grant, *J. Chem. Phys.* **84**, 3717 (1986).
38. S. J. Varner, R. L. Vold and G. H. Hoatson, *J. Magn. Reson. A* **123**, 72 (1996).
39. M. Bak and N. C. Nielsen, *J. Magn. Reson.* **125**, 132 (1997).
40. D. E. Goldberg, *Genetic Algorithms in Search, Optimization and Machine Learning*. Addison-Wesley, Reading, MA (1989).
41. Z. Michalewicz, *Genetic Algorithms + Data Structure = Evolution Programs*. Springer, Berlin (1992).
42. A. J. Keane, in *Modern Heuristic Search Methods*, edited by V. Rayward-Smith, I. Osman, C. Reeves and G. D. Smith. Wiley, New York (1996).
43. B. M. Kariuki, H. Serrano-González, R. L. Johnston and K. D. M. Harris, *Chem. Phys. Lett.* **280**, 189 (1997).
44. K. D. M. Harris, R. L. Johnston, B. M. Kariuki, *Acta Crystallogr., Sect. A* **54**, 632 (1998).

